Materials Research Express

PAPER

RECEIVED
17 March 2017

ACCEPTED FOR PUBLICATION
5 June 2017

PUBLISHED
3 August 2017

Simulation of Young's moduli for hexagonal ZnO [0 0 0 1]-oriented nanowires: first principles and molecular mechanical calculations

Andrei V Bandura[1], **Robert A Evarestov**[1], **Sergey I Lukyanov**[1], **Sergei Piskunov**[2] **and Yuri F Zhukovskii**[2,3]

[1] Quantum Chemistry Department, St. Petersburg State University, 7/9 Universitetskaya nab., St. Petersburg, 199034, Russia
[2] Institute of Solid State Physics, University of Latvia, Kengaraga 8, LV-1063, Riga, Latvia
[3] Author to whom any correspondence it to be addressed

E-mail: quantzh@latnet.lv

Keywords: wurtzite-structured ZnO (bulk and nanowires), *ab initio* hybrid PBE0 calculations (*CRYSTAL* code), force field calculations using pairwise potentials (*GULP* code), nanowire Young's modulus Y_{NW} and its dependence on diameter d_{NW}

Abstract

Morphologically reproducible wurtzite-structured zinc oxide nanowires (ZnO NWs) can be synthesized by different methods. Since ZnO NWs have been found to possess piezoelectricity, a comprehensive study of their mechanical properties, e.g. deformations caused by external compression or stretching, is one of the actual tasks of this paper. We have calculated wurtzite-structured [0 0 0 1]-oriented ZnO NWs whose diameters have been varied within 1–5 nm and 1–20 nm ranges when using either *ab initio* (hybrid DFT-LCAO) or force-field (molecular mechanical) methods, respectively (the minimum diameter d_{NW} of experimentally synthesized NWs has been estimated on average to be ~20 nm). When using both chosen calculation approaches, the values of Young's moduli determined for the mentioned ranges of NW diameters have been found to be qualitatively compatible (168–169 GPa for 5 nm NW thickness), whereas results of molecular mechanical simulations on Y_{NW} for 20 nm-thick NWs (160–162 GPa) have been qualitatively comparable with those experimentally measured along the [0 0 0 1] direction of NW loading. In all the cases, a gradual increase of the NW diameter has resulted in an asymptotic decrease of Young's modulus consequently approaching that (Y_b) of wurtzite-structured ZnO bulk along its [0 0 0 1] axis. The novelty of this study is that we combine the computation methods of quantum chemistry and molecular mechanics, while the majority of previous studies with the same aim have focused on the application of different classical molecular dynamical methods.

1. Introduction

Wurtzite-structured zinc oxide (ZnO) is not only a typical *n*-type semiconductor with a direct band gap of 3.3–3.4 eV but it also possesses a number of properties which can be used in key technological applications [1, 2], e.g. photocatalysis [3]. One of the most important applications is piezoelectricity, known as an effect of the electrical potential production (electron charge polarization) under external mechanical stress outside the crystal which does not possess central symmetry (e.g. *w*-ZnO) [4, 5]. Transformations of mechanical to electrical energy and vice versa are realized in a number of piezoelectric devices as well as in alternative electromechanical devices like micro-generators [6], transducers [7], actuators [8], etc, dealing with material elasticity and other mechanical properties. On the other hand, being reduced to nanoscale dimensions, for example, 2D nanothin films or 1D nanowires (NWs), the majority of materials can significantly change their behaviour compared with what they exhibit at macroscales (this also means, that bulk properties cannot be directly used for a proper description and modelling of the corresponding nanoscale systems). A variety of nanoelectromechanical systems based on NWs have been demonstrated recently [5, 9], where not only their mechanical properties have attracted enhanced interest but their tribological properties too (connected with friction, wear, adhesion and lubrication in nanoscale systems) although the latter has been significantly less studied so far.

Obviously, separately synthesized (not bundled) NWs, the shape and geometry parameters of which can be directly estimated using either atomic force microscopy [10] or inside a scanning electron microscope (SEM) [11], are quite attractive objects for nanotribomechanical studies [9], and can provide certain benefits as compared to

nanoparticles [10, 11]. Possessing one dimension outside the nanoscale, 1D NWs enable relatively easy location (some NWs are visible even in optical microscopes) and manipulation (dragging, pulling, bending, etc). The NW profile during manipulation on a substrate is determined by the balance between the elastic restoration forces inside the NW and the interaction between the NW and substrate [9]. If the NW geometry and elastic properties are known, an individual NW can serve as a self-sensing system while frictional forces can be extracted by observing the NW profile during manipulation.

Due to the structural anisotropy of ZnO NWs, their elastic properties were found to depend on both the orientation and cross-sectional diameter (d_{NW}) of individual NWs [9, 12–16]. On the other hand, experimental evaluations of the Young's modulus of ZnO NWs performed so far, diameters of which exceed 20 nm, have demonstrated a noticeable spread of Y_{NW} values within the range of 90–280 GPa [9]. ZnO NWs with a wide range of diameters (17–550 nm) and a uniform [0 0 0 1] growth orientation having wurtzite morphology of high quality single crystals were fabricated by a controllable thermal evaporation procedure [12]. Values of Y_{NW} measured within this range of NW diameters were decreased from 220 down to 140 GPa [13]. The buckling characterization by nanoindentation tests found that for $d_{NW} \approx 30$ nm, the value of Y_{NW} was estimated to be ~232 GPa while for $d_{NW} \approx 100$ nm, the Young's modulus was found to be 117 or 229 GPa depending on the experimental conditions [14]. Though the thinnest ZnO NW studied by Stan *et al* possessed $d_{NW} \approx 25.5$ nm [15], its Young's modulus was found to be higher by 38 GPa (19%) than that for $d_{NW} \approx 20$ nm from the experiment performed by Agrawal *et al* [16]. The most recent experimental study reveals that the Young's modulus equals ≈223 GPa for $d_{NW} \approx 20$ nm converging to $Y_{NW} \approx 115$ GPa for $d_{NW} > 40$ nm [9]. Meanwhile, the earlier reported experimental results obtained for the Y_b values of wurtzite-structured ZnO bulk crystal along its [0 0 0 1]-oriented axis were distributed in a range of values from 111.2 ± 4.7 GPa [2] up to 140 GPa [4]. A wide dispersion of Young's moduli values of ZnO measured for bulk and NWs of the same morphology using different methods indicates the necessity for their theoretical verification in order to clarify the reason for the large distinctions.

A number of theoretical simulations on the elastic properties of wurtzite-structured ZnO bulk and NWs have been performed so far. The authors of several studies have evaluated the dependence Y_{NW} (d_{NW}) of the ZnO-based NWs using simulations based on the classical molecular dynamics (MD) method within empirical force fields [16–20]. As is well-known, the classical MD technique provides a study of significantly larger systems as compared to the first principles DFT or *ab initio* MD. Nevertheless, the major part of the abovementioned works was restricted to relatively low-size samples. In particular, Kulkarni *et al* [17] have simulated the rectangular-sectioned ZnO nanobelts of [0 0 0 1], [0 1 $\bar{1}$ 0] and [2 $\bar{1}$ $\bar{1}$ 0] orientations with lateral dimensions of 1, 2 and 3 nm, for which the Y_{NW} values were evaluated. Dai and Park [18] as well as Wang *et al* [19] have simulated hexagonal-sectioned ZnO NWs, diameters of which have been changed from 0.85 to 4 nm. At the same time, Hu *et al* [20] have studied thicker NWs with diameters in the range of 1–10 nm, whereas Agrawal *et al* [16] applied the LAMMPS (large-scale atomic/molecular massively parallel simulator) classical MD code to model the Young's modulus of ZnO NWs as a function of NW diameters widely ranging from 5–20 nm. Additionally, an attempt to describe piezoelectricity in ZnO NWs with diameters up to 2.8 nm was undertaken using the first principles DFT method too [21]. Those calculations have indicated that the effective piezoelectric constant of ZnO NWs is larger than that of bulk ZnO, and it is saturated when the diameter of NWs exceeds 2.8 nm.

To verify the aforementioned results, we have consequently calculated wurtzite-structured [0 0 0 1]-oriented ZnO NWs whose diameters have been gradually varied within 1–5 nm or 1–20 nm ranges when using either *ab initio* (hybrid DFT-LCAO) or force-field (molecular mechanical) methods, respectively, whereas a minimum diameter d_{NW} of experimentally synthesized ZnO NWs has been estimated on average to be ~20 nm. Therefore, although first principles calculations of ZnO NWs do not allow us to compare the obtained results with data directly found experimentally, molecular mechanics fulfills the missing 5–20 nm gap, being comparable with both *ab initio* calculations and experiments. We have focused mainly on the evaluation of Young's moduli for ZnO NWs depending on the diameter of the NW and the comparison of Y_{NW} with Young's modulus of ZnO bulk along its [0 0 0 1] axis (Y_b).

The paper is organized as follows. The theoretical background (section 2) includes: a computational scheme for the evaluation of Young's moduli for 1D NWs and 3D bulk (2.1), atomistic models of wurtzite-structured ZnO bulk and [0 0 0 1]-oriented NWs (2.2), computational details of first principles hybrid DFT-HF calculations using the *CRYSTAL* code (2.3) as well as computational details of force-field molecular mechanical calculations using the *GULP* code (2.4). The results of calculations performed using both methods on equilibrium geometry and Young's modulus obtained for ZnO bulk (3.1) and NWs of different thicknesses (3.2) oriented along the [0 0 0 1] crystallographic axis are analyzed in section 3, including their comparison with the corresponding experimental and theoretical data available from the literature. The main conclusions are summarized in section 4.

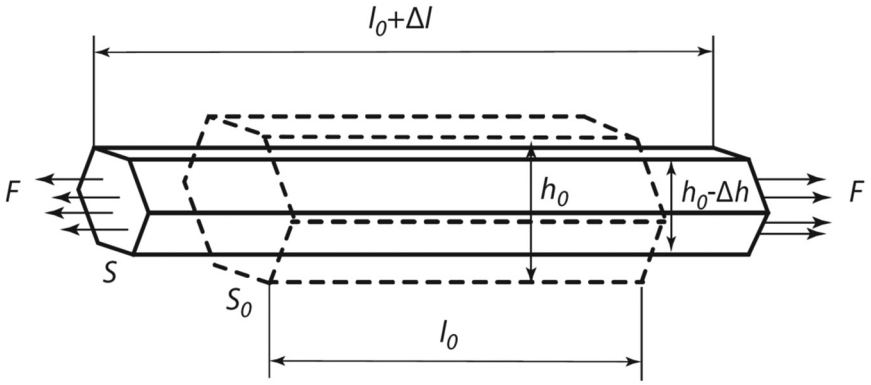

Figure 1. Initial (dotted) and stretched (solid) prisms corresponding to fragments of hexagonal wurtzite-structured rod before and after its mechanical loading along the [0 0 0 1]-oriented axis while h and h_0 are distances between the opposite facets of the prisms, respectively.

2. Theoretical background

2.1. Evaluation of Young's modulus

A simple model for the elasticity of a rigid rod was proposed earlier [22] where Young's modulus Y was appropriate to the case of uniaxial loading described using the following equation:

$$Y = \frac{\sigma}{\varepsilon_{\|}} = \frac{\sigma}{(\Delta l/l_0)}, \tag{1}$$

where $\sigma = F/S$ is the stress or force *per* unit area (where the force F acts along the chosen axis and S is its cross-sectional area, as shown in figure 1) while $\varepsilon_{\|} = \Delta l/l_0$ is the strain (fractional length change), where l_0 is the equilibrium length along the loading axis.

The loading force F is included in the total energy balance via the second order polynomial expression with a double differentiation of internal energy U [23], providing reliable conditions for the numerical evaluation of Young's modulus for rods (nanorods, Y_{NR}) at temperatures close to zero:

$$Y_{\mathrm{NR}} = \frac{1}{V_0}\left(\frac{\partial^2 U}{\partial \varepsilon_{\|}^2}\right)_{\varepsilon_{\|}=0}, \tag{2}$$

where $V_0 = S_0 \cdot l_0 = \sqrt{3}h_0^2 l_0/2$ is the volume of the unstrained system (figure 1). As a rule, both first principles and molecular mechanics simulations are related to zero temperature or values close to it ($T < 10$ K). To estimate Y values for NWs, we have employed the approximation based on equation (2) using specially-written codes to solve this equation by the polynomial presentation of the U function mentioned there (when performing either *ab initio* [24] or force-field [25] simulations).

Moreover, based on the theoretical simulations [26, 27] described below, we have analyzed the calculated Y_{b} values for wurtzite-structured ZnO bulk comparing them in table 1 with alternative data. (When using the Voigt–Reuss–Hill approach, Y_{b} was estimated to be 123.5 GPa [28], in qualitative agreement with bulk Young's modulus 144 GPa measured experimentally [4].) The value of Y_{b} for ZnO bulk loaded along the vertical [0 0 0 1] axis can be estimated via elastic constants c_{11}, c_{12}, c_{13} and c_{33} [26]:

$$Y_{\mathrm{b}} = c_{33} - \frac{2c_{13}^2}{c_{11} + c_{12}}. \tag{3}$$

2.2. Atomistic models of NWs

A conventional unit cell (UC) of wurtzite-structured ZnO bulk characterized by parameters a, c and u is imaged in figure 2. Its symmetry is described by the $P6_3mc$ space group [29]. In our first principles and force-field calculations, these values have been evaluated and verified by comparison with the corresponding experimental data (table 1).

The regular hexagonal prismatic shape of wurtzite-structured NWs synthesized in numerous experiments can be formed only if the NW axis is oriented along the hollow-centered [0 0 0 1] crystallographic direction [29], otherwise their symmetry is reduced while the stability is lowered. To better understand the structural and elastic properties of stoichiometric [0 0 0 1]-oriented six-faceted ZnO NWs of different diameters (figure 3), which can be cut from a host wurtzite-structured crystal, we have performed large-scale first principles calculations on each of them accompanied by total geometry optimization (table 2). The initial diameters of the ZnO NWs (d_{NW}) varied

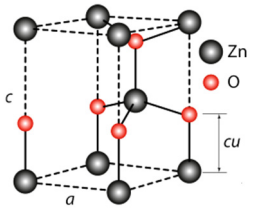

Figure 2. Axonometric image of ZnO conventional UC with enclosed labels (horizontal coordinates of atoms in the fifth layer coincide with those in the first layer). Solid lines correspond to Zn–O bonds.

from 0.98–4.90 nm which corresponds to a gradual extension of a hexagonal NW cross-section containing two (2 × 2) to eight (8 × 8) coordination cylinders arranged around a NW axis.

The latest edition of the *CRYSTAL* code [26] we used for *ab initio* calculations on ZnO NWs contains the new option NANOROD which, for the first time, allows users to generate 1D NWs of various structures when properly setting the chosen Miller indices of their lateral facets, simultaneously defining their crystallographic orientations. We recently checked the convenience of this approach when constructing [0 0 0 1]-oriented ZnO NWs with a hexagonal morphology [3]. The same algorithm of the ZnO NW construction has also been used for thin (figure 3) and relatively thick (figure 4) NWs calculated using the *GULP* code [27].

The symmetry of 1D wurtzite-structured and [0 0 0 1]-oriented ZnO NWs considered in this study can be described by the $P6_3mc$ rod group (corresponding to C_{6v}^4 space group) [30]. The stability of these NWs can be achieved while they are terminated by lateral facets possessing the smallest surface energy among any other wurtzite faces. This requirement can be fulfilled for a family of six identical $\{1\,\bar{1}\,0\,0\}$, $\{\bar{1}\,1\,0\,0\}$, $\{1\,0\,\bar{1}\,0\}$, $\{\bar{1}\,0\,1\,0\}$, $\{0\,1\,\bar{1}\,0\}$ and $\{0\,\bar{1}\,1\,0\}$ ZnO facets [29]. Figure 3 clearly shows that the structural optimization of the NWs results in the essential relaxation of external (facet) atomic layers while internal (core) atoms essentially remain in the regular cross-section positions, whereas their shifts along the NW axis are noticeably reduced with a growth of the NW diameter (table 2). This circumstance has been taken into account for the proper estimation of S_{NW} values (figure 1) to evaluate Y_{NW} depending on d_{NW} according to equation (2).

2.3. Details of first principles calculations

In this study, relaxed atomistic models of 1D ZnO NWs (figure 3) have been calculated using the periodic hybrid DFT-LCAO method based on the hybrid exchange–correlation functional PBE0 [31, 32]. This formalism implemented in the CRYSTAL14 computer code [26] utilizes the localized Gaussian-type functions (GTFs) in the form of a basis set (BS) centered on atomic nuclei for the expansion of crystalline orbitals as linear combinations of atomic orbitals. In the current study, we have used the all-valence BSs of atomic GTFs for both oxygen (constructed using pure *s*- and *d*- as well as hybrid *sp*-AOs in the form of 8*s*-411*sp*-1*d*) and zinc atoms (in the form of 8*s*-64111*sp*-41*d*) as suggested recently by Gryaznov *et al* [33].

To provide a balanced summation in both direct and reciprocal lattices, reciprocal space integration has been performed by sampling the NW's Brillouin zone (BZ) with 12 × 1 × 1 Pack–Monkhorst mesh [34] that gives in total 7 *k*-points evenly distributed along the BZ, which is a line section for periodically repeated 1D structures. Calculations are considered as converged only when the total energy differs by less than 10^{-10} a.u. in two successive cycles of the self-consistent field procedure. All the calculations have been performed with total geometry optimization keeping the symmetry fixed according to the $P6_3mc$ rod group. Within the self-consistency, the tolerances of $10^{-7}, 10^{-8}, 10^{-7}, 10^{-7}, 10^{-14}$ have been chosen for calculations of the Coulomb overlap, Coulomb penetration, exchange overlap, first exchange pseudo-overlap in direct space and second exchange pseudo-overlap in reciprocal space, respectively. To verify the chosen DFT-PBE0 computational scheme, we have compared the calculated lattice constants and elastic moduli of ZnO bulk with those measured experimentally (table 1).

To estimate Young's moduli for both ZnO bulk and [0 0 0 1]-oriented NWs calculated using the aforementioned first principles method, we have set the minimum of the anisotropic uniaxial (1D) or isotropic (3D) loadings equal to three (−1% for equilibrium structure compression, +1% for its stretching, and equilibrium structure *per se*). This minimum allows us to estimate the second derivative of internal energy function *U* and, correspondingly, Young's modulus Y_{NW} according to equation (2). In order to improve the precision of this procedure, we have tried to increase the number of loaded configurations (>3); however, this is rather problematic due to the marked expenditures of CPU time for the additional calculations. Moreover, values of Y_{NW} obtained for an increased number of configurations have been qualitatively close to those obtained for three configurations.

2.4. Details of molecular mechanical calculations

Dependences of Young's modulus of ZnO nanowire, Y_{NW}, on its diameter, d_{NW}, were estimated earlier using classical simulation methods [17–20]. The classical MD method based on the approach of empirical force fields

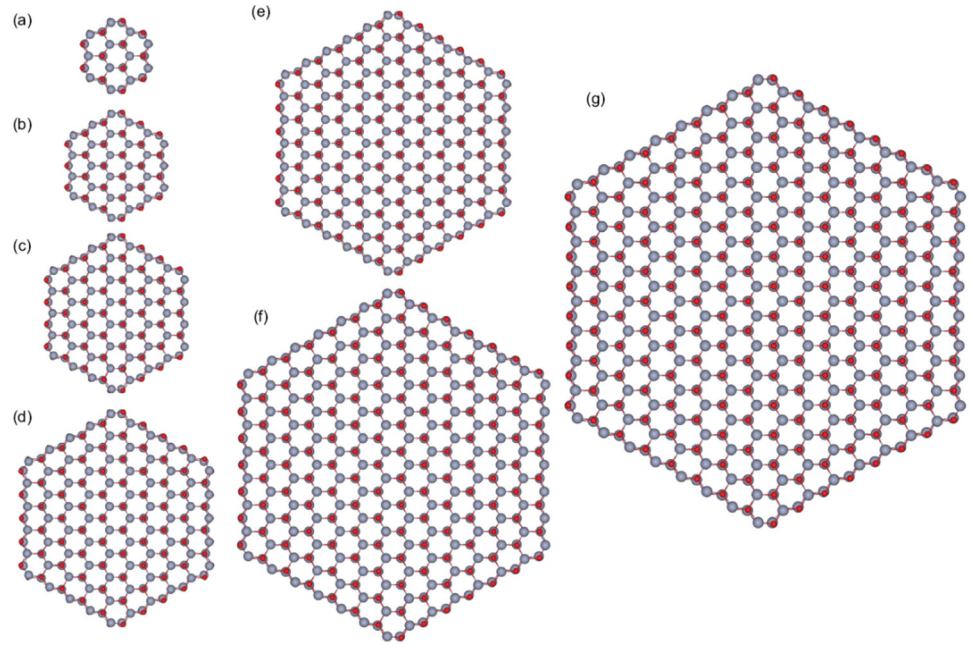

Figure 3. Cross sections of relaxed stoichiometric [0 0 0 1]-oriented ZnO NWs with different thicknesses given in table 2: (a) 2 × 2, (b) 3 × 3, (c) 4 × 4, (d) 5 × 5, (e) 6 × 6, (f) 7 × 7 and (g) 8 × 8 calculated using the *CRYSTAL*14 code. The small dark and middle-sized gray balls indicate O and Zn atoms, respectively. Obviously, the thinnest nanotube-like 1 × 1 nanoprism around the hollow-centered [0 0 0 1] axis contains six Zn and six O atoms *per* NW UC while arbitrary $n \times n$ NWs of ZnO contain $12n^2$ atoms *per* NW UC [3]. The value of d_{NW} is defined as the shortest distance between the opposite NW ribs.

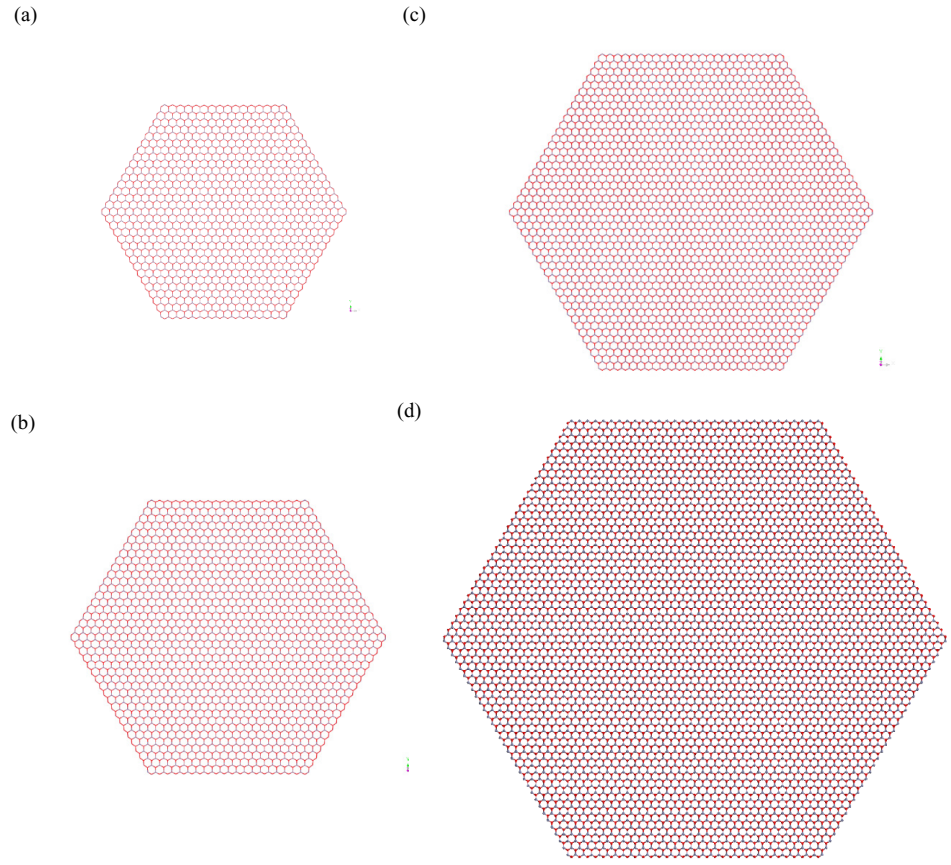

Figure 4. Cross sections of relaxed stoichiometric [0 0 0 1]-oriented ZnO NWs with different thicknesses given in table 2: (a) 16 × 16, (b) 20 × 20, (c) 24 × 24, and (d) 32 × 32 calculated using the *GULP* code.

was used for simulations on significantly larger atomistic systems as compared to those used for first principles DFT or *ab initio* MD simulations. Nevertheless, the majority of the aforementioned works was restricted to relatively thin samples, as mentioned in section 1. The force field of Binks [36, 37] was employed to perform MD simulations of ZnO NWs within the shell model, while their Young's moduli were obtained explicitly from the slope of the stress–strain curve [16–20]. MD calculations of stress based on the virial theorem formulated long ago [38] have been adapted recently for ZnO NWs by Lee *et al* [39].

In this study, we have employed the eight-parameter partially charged rigid ion model (PCRIM) recently proposed by Wang *et al* [40]. The PCRIM force field has a relatively simple functional form: a set of Born–Mayer potentials for short range interactions Zn–Zn and Zn–O, equation (4), as well as the Morse potential for O–O, equation (5), which includes seven pairwise parameters [40]:

$$E_{ij} = A_{ij} \cdot \exp(-r_{ij}/\rho_{ij}), \tag{4}$$

$$E_{ij} = -A_{ij} \cdot [(1 - \exp(-C_{ij} \cdot (r_{ij} - \rho_{ij})))^2 - 1], \tag{5}$$

where r_{ij} are the bond lengths while A_{ij}, C_{ij} and ρ_{ij} are the parameters (in eV, $Å^{-1}$ and Å, respectively) optimized for each type of pairwise interactions. The long range interactions of the ions possessing effective charges q_i and q_j are calculated according to the Coulomb law (equation (6)). The effective charge of Zn (1.14 e) is found to be the eighth parameter of the PCRIM model [40]:

$$E_{ij} = -q_i q_j / r_{ij}. \tag{6}$$

The experimentally observed and DFT-calculated lattice parameters of wurtzite-structured ZnO bulk are found to be in better agreement with the results provided by the PCRIM calculations (table 1) than those estimated using other force fields [41, 42]. Using a classical force field, the temperature effect on the thermodynamic, mechanical properties of the ZnO-based nanostructures can be investigated within quasi-harmonic approximation. The success of those investigations depends on how accurately the vibrational properties of ZnO bulk are reproduced using the interaction potential [43]. The PCRIM model has been recently applied in MD simulation [19] to calculate Y_{NW} and the yielding stress of the three thin ZnO NWs possessing $d_{NW} = 8.5, 15.6, 35.5$ Å.

The optimization of the atomic structure of the unstrained NW is the first step of Y_{NW} force field simulation. The period of the optimized structure l_0 (figure 1) corresponds to the minimal potential energy of the whole system. In order to obtain the dependence of the total internal energy U on the axial strain $\varepsilon_\parallel$, four contracted and eleven elongated samples have been considered: $l_i = l_0(1 + i\Delta\varepsilon_\parallel)$, where $i = -4, \ldots, 0, 1, \ldots, 11$. The strain step $\Delta\varepsilon_\parallel$ has a value of 9.53×10^{-4}. For each loaded sample, the period l_i has been fixed and a potential energy minimization procedure has been carried out to obtain the optimized atomic structure at the local minimum of the potential energy $E(\varepsilon_{\parallel,i}), \varepsilon_{\parallel,i} = i\Delta\varepsilon_\parallel = (l_i - l_0)/l_0$. A data set of 16 $E(\varepsilon_{\parallel,i})$ points has been obtained for each considered configuration of the ZnO NW. A five-degree polynomial was fitted to every total internal energy data set $E(\varepsilon_{\parallel,i})$. Differentiation of the polynomials allows one to calculate the second derivative of $E(\varepsilon_{\parallel,i})$ functions relative to tensile uniaxial strain $\varepsilon_{\parallel,i}$, according to equation (2).

3. Results of *ab initio* and molecular mechanical calculations of Young's moduli

3.1. Geometry and elastic properties of wurtzite-structured ZnO bulk

For verification of the *ab initio* hybrid DFT-PBE0 and force field RCRIM computational schemes, we have evaluated key properties of ZnO bulk (table 1). Equilibrium lattice constants and elastic moduli calculated for the wurtzite-structured ZnO bulk (using both *CRYSTAL* and *GULP* codes), the UC of which is imaged in figure 2, have been found in good qualitative agreement between themselves and with those estimated experimentally and theoretically. Firstly, it is true that for lattice constants, the theoretical and experimental estimates are very close. On the other hand, when using both methods, the calculated bulk moduli B of ZnO (according to its definition written at footnote of table 1) are noticeably lower than those measured experimentally, while the values of Young's modulus Y_b calculated by us according to Eq. (3) are essentially larger than the experimentally measured ones. Therefore, the comparison of the parameters given in table 1 allows us to conclude that both calculation methods can be used for the simulation of ZnO NWs.

3.2. Young's moduli evaluated for wurtzite-structured ZnO NW with varied d_{NW}

The key results of our large-scale calculations on ZnO NWs performed using *CRYSTAL* [26] and *GULP* [27] codes are summarized in table 2 and presented in figure 5 as plotted curves compared with the corresponding curves evaluated using MD simulations. According to equation (2) (section 2.1), Young's modulus strongly depends on the volume V_0 of an unstrained system. The cross section of a 1×1 hexagonal-shaped component from the center part of the $n \times n$ NW has an ideal hexagonal structure with $d_{NW} = 0.65$ nm. We have taken into account the fact

Table 1. Lattice constants a, c and u of ZnO crystal (figure 2) as well as bulk and Young's moduli B and Y_b, respectively, calculated by using hybrid DFT-PBE0 (*CRYSTAL*14) and PCRIM (*GULP*) methods as well as their comparison with available experimental and theoretical (mainly MD) data.

Parameter	*CRYSTAL* calculations	*GULP* calculations	Available experiment	Theoretical simulations
a, nm	0.326	0.324	0.325 [44]	0.321 [41]–0.329 [42]
c, nm	0.521	0.518	0.519 [44]	0.514 [36]–0.526 [41]
u	0.382	0.381	0.382 [35]	0.375 [41]–0.389 [36]
B[a], GPa	150.8	143.5	170–183 [45]	133.7 [36]–144.0 [42]
Y_b, GPa	167.7	167.4	111.2 [2]–144 [4]	123.5 [28]

[a] $B = \left(\frac{1}{2}\right)\left\{\left(\frac{1}{9}\right)[2(c_{11}+c_{12}) + 4c_{13}+c_{33}] + \frac{[(c_{11}+c_{12})c_{33}-2c_{13}^2]}{c_{11}+c_{12}+2c_{33}-4c_{13}}\right\}$, where c_{11}, c_{12}, c_{13} and c_{33} are elastic constants of wurtzite-structured ZnO bulk [46].

Table 2. Key parameters of optimized ZnO NWs (figures 3 and 4) evaluated using *GULP* and *CRYSTAL* codes.

			Force field calculations			First principles calculations		
$n \times n$ labels of ZnO NW cross-sections	Number of atoms n_{NW} *per* NW UC	Nanowire diameter d_{NW}, nm	l_{NW}[a], nm	$\left(\frac{\partial^2 U}{\partial \varepsilon_{\parallel}^2}\right)$, eV	Y_{NW}, GPa	l_{NW}[a], nm	$\left(\frac{\partial^2 U}{\partial \varepsilon_{\parallel}^2}\right)$, eV	Y_{NW}, GPa
2 × 2	48	0.98	0.525	446	206.2	0.534	511	232.2
3 × 3	108	1.63	0.521	1067	186.9	0.529	1181	203.5
4 × 4	192	2.29	0.520	2000	180.9	0.526	2129	190.3
5 × 5	300	2.94	0.519	3228	177.4	0.525	3367	183.0
6 × 6	432	3.59	0.519	4752	175.2	0.524	4895	178.6
7 × 7	588	4.25	0.519	6559	173.3	0.524	6725	176.0
8 × 8	768	4.90	0.519	8666	172.2	0.523	8816	173.6
16 × 16	3072	10.10	0.518	36 119	168.3	—	—	—
20 × 20	4800	12.70	0.518	56 907	167.6	—	—	—
24 × 24	6912	15.30	0.518	82 407	167. 2	—	—	—
32 × 32	12 288	20.50	0.518	147 533	166.6	—	—	—
Bulk	—	—	—	—	167.4	—	—	167.7

[a] l_{NW} is the length of a NW UC.

that, in the case of 2 × 2 and 3 × 3 NWs, the number of the terminating 1 × 1 components is greater than the number of those inside the NW, unlike thicker NWs. In table 2, we separately show parameters of equation (2).

In accordance with table 2 and figure 5, the maximum discrepancy between the Young's modulus evaluated using DFT-PBE0 and the PCRIM force field method is observed for a 2 × 2 ZnO NW cross-section (its difference achieves 13%). With an increasing d_{NW} value, this discrepancy is essentially reduced (down to 0.8% for $d_{NW} = 4.9$ nm). A similar trend is observed when comparing the Young's modulus obtained in our force field calculations and MD simulations performed earlier by Agrawal *et al* [16] in the asymptotic plot area at $d_{NW} \approx 20$ nm (figure 5) where the difference in the corresponding Y_{NW} values is about 2%, although at d_{NW} approaching 5 nm it achieves 12%. In any case, we can suggest that a further increase of d_{NW} can result in a gradual approach of Y_{NW} to Y_b. As to values of Young's modulus calculated at small d_{NW} (<1 nm), when comparing our force field and MD results obtained by Wang *et al* [19], they are too large (with a discrepancy up to 50%), although in this case d_{NW} growth leads to a marked decrease of Y_{NW} (figure 5). On the other hand, the results of the MD simulations obtained by Hu *et al* [20] are very close to the MD data extracted from [16] for d_{NW} in the range of 5–10 nm (4%, 0.4% and 2% for NW diameters 5.3 nm, 7.6 nm and 10.0 nm, respectively). For the thinnest NW 3 × 3 (1.63 nm), the value of Young's modulus estimated by Hu *et al* approaches the corresponding *ab initio* result (its difference does not exceed 4%, as shown in figure 5). On the whole, values of Y_{NW} evaluated using quantum chemistry, molecular mechanical and molecular dynamical methods are found to be qualitatively close.

At the same time, if a spread of Y_{NW} (d_{NW}) curve distributions evaluated theoretically (figure 5) is noticeable (due to different methods of calculations and their parameters), then a similar spread of experimental measurements is markedly larger (see figures 5 and 6). Obviously, this difference is caused not only by principally different methods of NW synthesis and arrangement but also by a variety of techniques used for Young's modulus measurement (uniaxial tensile test, cantilevered beam bending, 3-point bending, resonance method, nanoindentation, buckling test, etc) [9, 12–16, 47–50]. The reported experimental results for the Young's modulus of the wurtzite ZnO bulk crystal oriented along [0 0 0 1] are also distributed in a range of values (110–140 GPa) [2, 4].

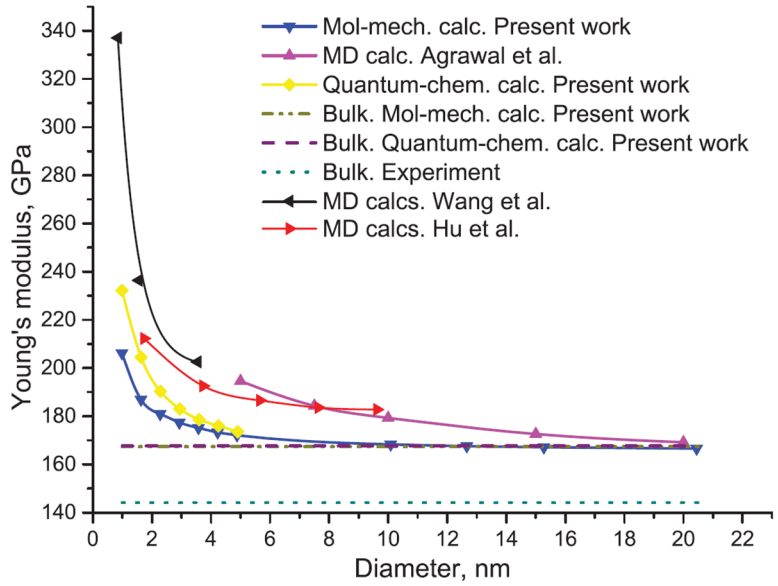

Figure 5. Dependence of Young's moduli on NW diameters Y_{NW} (d_{NW}) calculated using *GULP* and *CRYSTAL* computational codes (blue and yellow plotted curves, respectively) following the results presented in table 2. Additionally, the Y_{NW} (d_{NW}) plot presents MD curves adopted from [16, 19, 20] (magenta, black and red curves, respectively) as well as coinciding dash-dot horizontal lines corresponding to Y_b of the wurtzite-structured ZnO bulk evaluated by *ab initio* and force field methods. The dotted green line at the bottom corresponds to experimentally measured bulk Young's modulus [4].

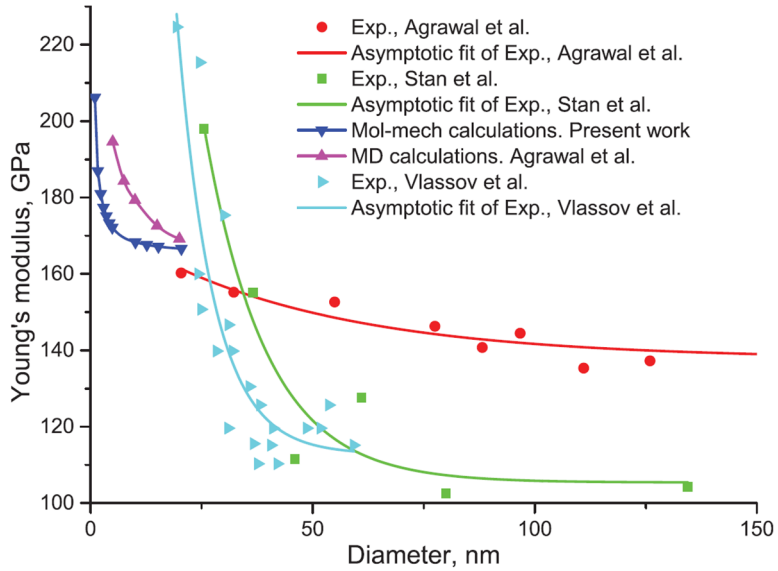

Figure 6. Y_{NW} (d_{NW}) curves drawn using an asymptotic fit of Young's moduli experimentally measured by Vlassov *et al* [9] (pale blue), Stan *et al* [15] (pale green) and Agrawal *et al* [16] (red) compared with the results obtained using our force field calculations (blue) and MD calculations by Agrawal *et al* [16] (magenta).

Both quantum chemistry and molecular mechanics calculations in this study have been performed for 0 K and no thermodynamic treatment of their results has been conducted. On the other hand, the majority of the experimental measurements of Y_{NW} have been carried out at room temperature (*RT*) only, which is perhaps an alternative reason for the differences in describing Young's modulus as observed in figure 5. MD simulations can also be performed for a wide temperature interval, e.g. *RT* [16, 19, 20]. However, several attempts have already been undertaken in order to describe, theoretically, a trace behavior of Young's modulus in a large temperature interval, including recent molecular mechanical simulations of $Y_{NT}(T)$ and $Y_{NW}(T)$ for anatase-structured titania nanotubes and rutile-structured TiO_2 NWs, respectively [25], which were performed using the *GULP* code [27]. It has been shown that values of Y_{NT} for TiO_2 NTs decrease by 4%–6% (depending on d_{NT}) in the temperature interval [0, *RT*]: the thicker the NT, the larger the value of ΔY_{NT} is obtained. This can be considered as one reason for the difference between the experimental and theoretical values (for example, Y_{NW} of ZnO bulk—table 1 and figure 5). Nevertheless, this is not so crucial for qualitative comparison of simulated and measured values of elasticity.

4. Conclusions

Molecular mechanical simulations combined with first principles DFT-PBE0 calculations allow us to predict the behavior of the Young's modulus of ZnO NWs in a wide range of NW diameters (0.5–20.5 nm) whereas experimental measurements can be performed for $d_{NW} \geqslant 20$ nm. Thus, we have achieved a complete overlap between the intervals of NW sizes necessary for the evaluation of Y_{NW}. Taking into account the high level of uncertainty demonstrated by the experimental measurements of the ZnO NWs' elastic properties, the results of our molecular mechanics simulations may indicate the most probable size dependence of the Young's modulus of ZnO NWs. Moreover, the qualitative coincidence of Y_{NW} (d_{NW}) constructed on the basis of combined first principles and force field calculations allow us to predict the electronic properties of ZnO NW diameters which exceed 5 nm. Our large-scale *ab initio* evaluation of Young's moduli for ZnO NWs has been one of the first attempts which can be explained by extreme CPU expenditures necessary for the reliable performance of such calculations.

The qualitative proximity of Y_{NW} (d_{NW}) curves calculated using molecular mechanical and molecular dynamical methods is important since the majority of the theoretical simulations on Young's moduli for ZnO NWs performed so far have been based on the formalism of classical MD. The qualitative coincidence between the results of the theoretical simulations and experimental measurements is rather problematic due to a large spread of Y_{NW} values depending on NW diameters. Our alternative theoretical approaches can help to overcome uncertainty in the interpretation of the experimental results.

The evaluation of Y_b for ZnO bulk is necessary in order to estimate the asymptotic limit for the Young's modulus of NWs, which can be achieved during the gradual growth of d_{NW}. The length of a ZnO NW UC is gradually reduced with increasing d_{NW} achieving a certain asymptotic limit. Simultaneously, relative NW reconstruction (mainly its external shell) is reduced with d_{NW} growth.

Acknowledgments

The authors thank A Gulans, B Polyakov and S Vlassov for stimulating discussions. This study has been supported by the ERA.Net RUS Plus project No. 237 Watersplit. AB, RE and SL acknowledge the financial support by the Russian Foundation for Basic Research (Grant No. 17-03-00130-a) and the assistance of the Saint Petersburg State University Computer Center in the accomplishment of high-performance computations.

References

[1] Janotti A and Van de Walle C G 2009 Fundamentals of zinc oxide as a semiconductor *Rep. Prog. Phys.* **72** 126501
[2] Kucheyev S O, Bradby J E, Williams J S, Jagadish C and Swain M V 2002 Mechanical deformation of single-crystal ZnO *Appl. Phys. Lett.* **80** 956–8
[3] Zhukovskii Yu F, Piskunov S, Lisovski O, Spohr E and Evarestov R A 2016 Quantum chemical simulations of doped ZnO nanowires for photocatalytic hydrogen generation *Phys. Status Solidi* b **253** 2120–8
[4] Wern H 2004 *Single Crystal Elastic Constants and Calculated Bulk Properties: a Handbook* (Berlin: Logos Verlag)
[5] Wang Z L 2010 Piezopotential gated nanowire devices: piezotronics and piezo-phototronics *Nano Today* **5** 540–52
[6] Pan C T, Liu Z H, Chen Y C and Liu C F 2010 Design and fabrication of flexible piezo-microgenerator by depositing ZnO thin films on PET substrates *Sensors Actuators* A **159** 96–104
[7] Laurenti M, Perrone D, Verna A, Pirri C F and Chiolerio A 2015 Development of a flexible lead-free piezoelectric transducer for health monitoring in the space environment *Micromachines* **6** 1729–44
[8] Muralt P, Polcawich R and Trolier-McKinstry S 2009 Piezoelectric thin films for sensors, actuators, and energy harvesting *MRS Bull.* **34** 658–64
[9] Vlassov S, Polyakov B, Oras S, Vahtrus M, Antsov M, Šutka A, Smits K, Dorogin L M and Lõhmus R 2016 Complex tribomechanical characterization of ZnO nanowires: nanomanipulations supported by FEM simulations *Nanotechnology* **27** 335701
[10] Dietzel D, Monninghoff T, Jansen L, Fuchs H, Ritter C, Schwarz U D and Schirmeisen A 2007 Interfacial friction obtained by lateral manipulation of nanoparticles using atomic force microscopy techniques *J. Appl. Phys.* **102** 12–7
[11] Polyakov B, Vlassov S, Dorogin L M, Butikova J, Antsov M, Oras S and Lõhmus R 2014 Manipulation of nanoparticles of different shapes inside a scanning electron microscope *Beilstein J. Nanotechnol.* **5** 133–40
[12] Zhang Y, Wang L, Liu X, Yan Y, Chen C and Zhu J 2005 Synthesis of nano/micro zinc oxide rods and arrays by thermal evaporation approach on cylindrical shape substrate *J. Phys. Chem.* B **109** 13091–3
[13] Chen C Q, Shi Y, Zhang Y S, Zhu J and Yan Y J 2006 Size dependence of Young's modulus in ZnO nanowires *Phys. Rev. Lett.* **96** 075505
[14] Ji L W, Young S J, Fang T H and Liu C H 2007 Buckling characterization of vertical ZnO nanowires using nanoindentation *Appl. Phys. Lett.* **90** 033109
[15] Stan G, Ciobanu C V, Parthangal P M and Cook R F 2007 Diameter-dependent radial and tangential elastic moduli of ZnO nanowires *Nano Lett.* **7** 3691–7
[16] Agrawal R, Peng B, Gdoutos E E and Espinosa H D 2008 Elasticity size effects in ZnO nanowires: a combined experimental-computational approach *Nano Lett.* **8** 3668–74
[17] Kulkarni A J, Zhou M and Ke F J 2005 Orientation and size dependence of the elastic properties of zinc oxide nanobelts *Nanotechnology* **16** 2749–56
[18] Dai S and Park H S 2013 Surface effects on the piezoelectricity of ZnO nanowires *J. Mech. Phys. Solids* **61** 385–97
[19] Wang W, Pi Z, Lei F and Lu Y 2016 Understanding the tensile behaviors of ultra-thin ZnO nanowires via molecular dynamics simulations *AIP Adv.* **6** 035111

[20] Hu J, Liu X W and Pan B C 2008 A study of the size-dependent elastic properties of ZnO nanowires and nanotubes *Nanotechnology* **19** 285710
[21] Xiang H J, Yang J, Hou J G and Zhu Q 2006 Piezoelectricity in ZnO nanowires: a first-principles study *Appl. Phys. Lett.* **89** 223111
[22] Ledbetter H M and Naimon E R 1974 Elastic properties of metals and alloys. II. Copper *J. Phys. Chem. Ref. Data* **3** 897–935
[23] Griebel M, Hamaekers J and Heber F 2009 A molecular dynamics study on the impact of defects and functionalization on the Young modulus of boron–nitride nanotubes *Comput. Mater. Sci.* **45** 1097–103
[24] Gulans A and Tale I 2007 *Ab initio* calculation of wurtzite-type GaN nanowires *Phys. Status Solidi* c **4** 1197–2000
[25] Lukyanov S I, Bandura A V and Evarestov R A 2016 Young's modulus and Poisson's ratio for TiO_2-based nanotubes and nanowires: modelling of temperature dependence *RSC Adv.* **6** 16037–45
[26] Dovesi R *et al* 2014 *CRYSTAL14 User's Manual* (Turin: University of Torino)
[27] Gale J D 2011 *General Utility Lattice Program GULP* (Perth: Curtin University)
[28] Chung D H and Buessem W R 1968 The Voigt–Reuss–Hill (VRH) approximation and the elastic moduli of polycrystalline ZnO, TiO_2 (rutile), and -Al_2O_3 *J. Appl. Phys.* **39** 2777–82
[29] Evarestov R A 2015 *Theoretical Modeling of Inorganic Nanostructures. Symmetry and Ab Initio Calculations of Nanolayers, Nanotubes and Nanowires* (*NanoScience and Technology*) (Berlin: Springer)
[30] Milošević I, Stevanović V, Tronc P and Damnjanović M 2006 Symmetry of zinc oxide nanostructures *J. Phys.: Condens. Matter* **18** 1939–53
[31] Perdew J P, Ernzerhof M and Burke K 1996 Non-local exchange and correlation *J. Chem. Phys.* **105** 9982–5
[32] Adamo C and Barone V 1999 Toward reliable density functional methods without adjustable parameters: the PBE0 model *J. Chem. Phys.* **110** 6158–79
[33] Gryaznov D, Blokhin E, Sorokin A, Kotomin E A, Evarestov R A, Bussmann-Holder A and Maier J 2013 A comparative *ab initio* thermodynamic study of oxygen vacancies in ZnO and $SrTiO_3$: emphasis on phonon contribution *J. Phys. Chem.* C **117** 13776–84
[34] Monkhorst H J and Pack J D 1976 Special points for Brillouin-zone integrations *Phys. Rev.* B **13** 5188–92
[35] Usseinov A B, Kotomin E A, Akilbekov A T, Zhukovskii Yu F and Purans J 2014 Hydrogen induced metallization of ZnO (1 $\bar{1}$ 0 0) surface: *ab initio* study *Thin Solid Films* **553** 38–42
[36] Binks D J 1994 Computional modelling of zinc oxide & related oxide ceramics *PhD Thesis* University of Surrey, Harwell, United Kingdom
[37] Grimes R W, Binks D J and Lidiard A B 1995 The extent of zinc oxide solution in zinc chromate spinel *Phil. Mag.* A **72** 651–68
[38] Allen M P and Tildesley W J 1989 *Computer Simulation of Liquids* (Oxford: Oxford University Press)
[39] Lee W J, Chang J G, Ju S P, Weng M H and Lee C H 2011 Structure-dependent mechanical properties of ultrathin zinc oxide nanowires *Nanoscale Res. Lett.* **6** 352
[40] Wang S, Fan Z, Koster R S, Fang C, van Huis M A, Yalcin A O, Tichelaar F D, Zandbergen H W and Vlugt T J H 2014 New *ab initio* based pair potential for accurate simulation of phase transitions in ZnO *J. Phys. Chem.* C **118** 11050–61
[41] Erhart P, Juslin N, Goy O, Nordlund K, Műller R and Albe K 2006 Analytic bond-order potential for atomistic simulations of zinc oxide *J. Phys.: Condens. Matter* **18** 6585–605
[42] Raymand D, van Duin A C T, Baudin M and Hermansson K 2008 A reactive force field (ReaxFF) for zinc oxide *Surf. Sci.* **602** 1020–31
[43] Serrano J, Manjón F J, Romero A H, Ivanov A, Cardona M, Lauck R, Bosak A and Krisch M 2010 Phonon dispersion relations of zinc oxide: inelastic neutron scattering and *ab initio* calculations *Phys. Rev.* B **81** 174304
[44] Albertsson J, Abrahams S C and Kvick A 1989 Atomic displacement, anharmonic thermal vibration, expansivity and pyroelectric coefficient thermal dependences in ZnO *Acta Cryst.* B **45** 34–40
[45] Karzel H *et al* 1996 Lattice dynamics and hyperfine interactions in ZnO and ZnSe at high external pressures *Phys. Rev.* B **53** 11425–38
[46] Tan J, Li Y and Ji G 2012 Elastic constants and bulk modulus of semiconductors: performance of plane-wave pseudopotential and local-density-approximation density functional theory *Comput. Mater. Sci.* **58** 243–7
[47] Soomro M Y, Hussain I, Bano N, Broitman E, Nur O and Willander M 2012 Nanoscale elastic modulus of single horizontal ZnO nanorod using nanoindentation experiment *Nanoscale Res. Lett.* **7** 146
[48] Song J, Wang X, Riedo E and Wang Z L 2005 Elastic property of vertically aligned nanowires *Nano Lett.* **5** 1954–8
[49] Hoffmann J S, Östlund F, Michler J, Fan H J, Zacharias M, Christiansen S H and Ballif C 2007 Fracture strength and Young's modulus of ZnO nanowires *Nanotechnology* **18** 205503
[50] Asthana A, Momeni K, Prasad A, Yap Y K and Yassar R S 2011 *In situ* observation of size-scale effects on the mechanical properties of ZnO nanowires *Nanotechnology* **22** 265712

Institute of Solid State Physics, University of Latvia as the Center of Excellence has received funding from the European Union's Horizon 2020 Framework Programme H2020-WIDESPREAD-01-2016-2017-TeamingPhase2 under grant agreement No. 739508, project CAMART²